J Porous Mater
DOI 10.1007/s10934-011-9537-y

Effect of particle morphology and pore size on the release kinetics of ephedrine from mesoporous MCM-41 materials

Dua'a M. Marzouqa · Mohammad B. Zughul · Mutasem O. Taha · Hamdallah A. Hodali

Abstract Ephedrine was loaded onto siliceous mesoporous materials of different pore sizes, and the corresponding drug release into simulated body fluid at pH 7.4 and 37 °C was measured against time over a period of 72 h. The mesoporous materials designated MCM-41(C_N) were prepared at different pore sizes using a self-assembly mechanism. The pore size was controlled by the use of alkyltrimethylammonium bromide (C_NTAB) surfactants having different alkyl chain lengths (C_{10}, C_{12}, and C_{14}). The three mesoporous materials showed good ephedrine-loading capacities from dry ethanolic solutions, which slightly increased with the pore size of MCM-41(C_N). From the drug release profiles, the overall release of ephedrine followed the order: MCM-41(C_{12}) > MCM-41(C_{14}) > MCM-41(C_{10}), with the release of ephedrine attaining 92% of the drug load from MCM-41(C_{12}). Ephedrine release approached 60% of the drug load in 6 h and 92% in 20 h. The results of in vitro release kinetics indicate that pore size is not the only factor affecting ephedrine release, but also pore channel length and overall particle morphology.

Keywords Drug delivery · Ephedrine · MCM-41 · Mesoporous materials

D. M. Marzouqa · M. B. Zughul · H. A. Hodali (✉)
Department of Chemistry, Faculty of Sciences, University of Jordan, Amman 11942, Jordan
e-mail: h-hodali@ju.edu.jo

M. O. Taha
Drug Discovery Unit, Department of Pharmaceutical Sciences, Faculty of Pharmacy, University of Jordan, Amman 11942, Jordan

Abbreviations

SBF	Simulated body fluid
C_NTMB	Alkyltrimethylammonium bromide
MCM-41	Mobil crystalline material no. 41
DW	Deionized water

1 Introduction

The synthesis of a new family of silica-based mesoporous materials in the early nineties [1, 2], designated as MCM-41 (Mobil Crystalline Material number 41), indicated a great potential for new applications involving relatively bulk molecules [3]. This class of mesporous materials possesses uniformly organized porous structures, which comprise hexagonally arranged channels having diameters between 1.5 and 10 nm [4]. These systems exhibit some favorable physical properties that have attracted the attention of scientists, including their highly ordered structures, very high specific surface areas, adaptability to pore size control, and moderate thermal and hydrothermal stabilities. With these unique features, members of MCM-41 are regarded as good materials for hosting drug molecules of several sizes, shapes and functionalities, and are thus advocated for utilization as drug delivery vehicles [5].

Inorganic microporous and mesoporous materials based on clays and silica have shown adequate and, in some cases, favorable physical characteristics [5, 6]. Several research groups have utilized the highly ordered mesoporus material MCM-41 as a drug delivery system. Examples of the drugs that have been studied are: aspirin [7], atenolol [8], captopril [9], coumarin derivatives [10], diflunisal [11], hydrochlorothazide [12], ibuprofen [4, 5, 13–16], methotrexate [17], naproxine [13], and sertraline hydrochloride

Published online: 04 December 2011

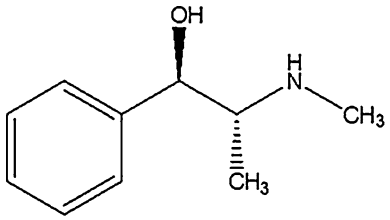

Fig. 1 Structure of the ephedrine isomer used which is (1R,2S)-(−)-ephedrine

[18]. The results of these studies are very promising, especially with regards to applications involving drug sustained release. However, considerable research work is still needed to explore the various modes of interactions involved between the mesoporous host matrix and the guest drug molecules, especially in relation to their effect on drug loading and drug sustained release.

Herein, we report on the preparation of the siliceous MCM-41 with different pore diameters employing alkyltrimethylammonium bromide surfactants having different alkyl chain lengths (C_{10}, C_{12}, and C_{14}). Physical characterization of the prepared mesoporous materials was conducted using XRD and SEM, in addition to N_2 adsorption/desorption measurements and BET analysis for specific surface areas. Samples of the synthesized siliceous materials were loaded with free ephedrine (Fig. 1), and the corresponding in vitro release profiles into simulated body fluid (SBF) were measured at pH 7.4 and 37 °C over a period of 72 h. The results of release kinetics, which were obtained through rigorous analysis of the experimental data using different release models, are also reported and discussed.

Ephedrine is a natural alkaloid isolated from *Ephedra sinica* herbs which grow mainly in the northeast and northwest regions of China. The herb has been used as a Chinese folk medicinal for a long time. Ephedrine is a central nervous system stimulant, which has been utilized in the treatment of several human ailments. For example, it is used as a bronchodilator, as a nasal decongestant, in the treatment of orthostatic hypotension as well as other diseases [19]. Ephedrine was selected as a model drug for this study for two reasons: first for its molecular size which is suitable for loading into mesoporous materials, especially MCM-41, and second for exploring the possibility of attaining sustained ephedrine release, over an extended period of time, due to the hazardous side effects accompanying an otherwise fast ephedrine release [20].

2 Experimental

2.1 Materials and methods

(1R,2S)-(−)-Ephedrine hydrochloride and dodecyltrimethylammonium bromide were obtained from Aldrich Chimica. Decyltrimethylammonium bromide, tetradecyltrimethylammonium and tetraethylorrthosilane were obtained from Acros, USA. The above chemicals were used as received. Solvents were dried by standard procedures. Deionized water (DW) was used throughout. Simulated body fluid at pH 7.4 was prepared following an earlier procedure [21] with some modification. X-ray powder diffraction spectra were measured using a Philips 2 kW model x-ray diffractometer (Cu-Kα radiation source at $\lambda = 1.5418$ Å) at a scan rate of 2°/min. Specific surface areas and pore size distributions were estimated through BET modeling using a nitrogen adsorption/desorption instrument (Nova 2200e). FTIR spectra (4,000–400 cm^{-1}, 4 cm^{-1} spectral resolution, KBr pellets) were measured using a Thermo Nicolet NEXUS 670 FT-IR spectrometer. UV–Visible spectra were recorded using a Cary 100 Bio UV–Visible spectrophotometer (Varian). Thermal gravimetric analysis (TGA) was conducted using a Netzsch Sta 409 PC instrument (NETZSCH-Ger). The morphologies of the solid samples were monitored by scanning electron microscopy (SEM) using an FEI-FEG INSPEC F50 instrument.

2.2 Synthesis of MCM-41 samples

Samples of the mesoporous silicious MCM-41 of different pore sizes were prepared following an earlier procedure [22] with some modification: 5.60 mmol of the appropriate alkyltrimethylammonium bromide surfactant (with C_{10}, C_{12} or C_{14} alkyl chain length) were dissolved in DW (122 mL). To this solution, 8.0 g of ammonia solution (25.0%) were added and the mixture was stirred for 10 min. Following this, 10.0 g of tetraethylorthosilicate were added dropwise with vigorous stirring till the addition was complete, then stirring was continued for 4 h. The solid precipitate formed was filtered, washed with DW and dried at 110 °C for 12 h. The mesoporous material was then calcined at 540 °C for 6 h in air to remove the surfactant template. These calcined solid products, which were obtained using the C_{10}, C_{12}, and C_{14} surfactant templates were respectively denoted as MCM-41(C_{10}), MCM-41(C_{12}) and MCM-41(C_{14}).

2.3 Drug loading and release

Loading was started with the liberation of (−)-ephedrine from the corresponding hydrochloride salt by reaction with sodium ethoxide in dry ethanol. To a round-bottomed flask containing 100.0 mL dry ethanol, sodium (0.70 g, 0.030 mol) was added in small pieces under nitrogen atmosphere. As the reaction of sodium ceased, (−)-ephedrine.HCl (6.00 g, 0.030 mol) was added and the solution was stirred for 15 min

under nitrogen. To 50 mL of a filtered solution of (−)-Ephedrine, 1.50 g of MCM-41 were added and the mixture was stirred at room temperature for 24 h. The loaded material was filtered, washed with dry ethanol and dried in vacuum. A blank sample was prepared by stirring MCM-41 (1.50 g) in dry ethanol (50 mL) at room temperature for 24 h, and then treated as above. The loading capacity of the drug was determined from the initial and final concentrations of (−)-ephedrine in ethanol solution, which were measured UV–Visible absorption spectrophotometry. Absorbances were measured at 256 nm and concentrations were estimated against a calibration curve of ephedrine in ethanol at 25 °C.

Samples of the drug-loaded material (0.30 g each) were pressed under pressure (∼60 MPa) into discs (2.5 × 13 mm). Each disc was soaked in 250.0 mL of SBF solution at pH 7.4 and 37 °C and left continuously stirred in a thermostated bath shaker for 72 h. Filtered samples (2.50 mL esch) were withdrawn at the time intervals 1.5, 3.0, 4.5, 6.0, 7.5, 24, 33, 48, 56, and 72 h. The molar concentrations of ephedrine released into these samples were estimated from the corresponding absorbances measured at 257 nm against a calibration curve of ephedrine in SBF buffer at pH 7.4 and 37 °C.

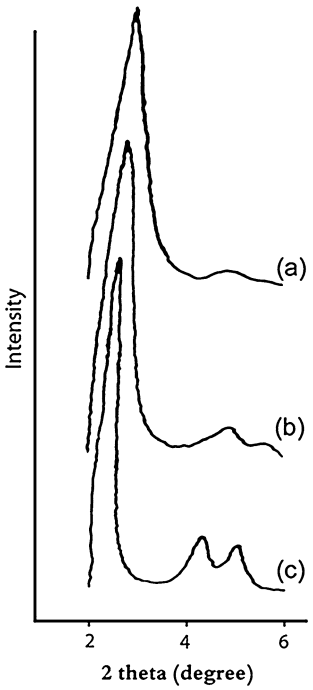

Fig. 2 XRD spectra of the mesoporous materials: **a** MCM-41(C_{10}), **b** MCM-41(C_{12}) and **c** MCM-41(C_{14})

3 Results and discussion

3.1 Characterization of mesoporous materials

The powder X-ray diffraction patterns of the MCM-41(C_N) samples prepared for C_{10}, C_{12} and C_{14} are depicted in Fig. 2. The corresponding patterns are characteristic of mesoporous materials, which normally exhibit a very intense peak at low angle corresponding to (100) reflections, in addition to the weak broad peaks at higher angles. Estimates of the 100 planes distances (d, nm) are listed in Table 1 for MCM-41(C_{10}), MCM-41(C_{12}) and MCM-41(C_{14}).

FTIR spectra were measured for MCM-41 samples over the range 4000 to 400 cm^{-1} using a KBr pellets at a spectral resolution of 4 cm^{-1}. Each sample was heated to 60 °C in a vacuum oven overnight prior to FTIR measurement. Figure 3 depicts the spectrum corresponding to MCM-41(C_{10}), which was typical of mesoporous MCM-41 materials exhibiting the MCM-41 characteristic prominent bands. These bands were thoroughly checked with the related literature [23–30] and were properly assigned. For example, the presence of free surface silanaol hydroxyl (Si–O–H) groups was ascertained by the characteristic stretching vibration at 3,743 cm^{-1}. Si–O bond stretching and Si–O rocking vibrations of surface Si–O–H groups were also evident at 967 and 460 cm^{-1}, respectively. The very broad (hydrogen-bonded) hydroxyl stretching band for both silanol Si–O–H and water hydroxyls was apparent at 3415 cm^{-1}, in addition to the characteristic water H–O–H twisting band at 1,633 cm^{-1}. Moreover, the surface (external) Si–O–Si asymmetric stretching vibration at 1238 cm^{-1}, the internal Si–O-Si stretching vibrations (SiO_4 asymmetric at 1,084 cm^{-1} and symmetric at 802 cm^{-1}) were all very clearly evident (Fig. 3). No significant variation among the IR bands of the three mesoporous materials was observed.

The nitrogen adsorption/desorption isotherms measured for the three MCM-41(C_N) materials are shown in Fig. 4. The curves correspond to a type IV isotherms (IUPAC classification), which are typical of mesoporous materials. Estimates of the surface areas (S_{BET}, m^2/g), pore volumes (V, cm^3/g) and average pore sizes (D_p, nm) corresponding to MCM-41(C_{10}), MCM-41(C_{12}) and MCM-41(C_{14}) are listed in Table 1.

The morphologies of MCM-41(C_{10}) and MCM-41(C_{12}), which are depicted by the SEM micrographs in Fig. 5, indicate spherical particles with average diameters of 1.1 and 0.8 μm, respectively. In contrast, the SEM micrograph of MCM-41(C_{14}) depicts irregularly-shaped rods with an average length of 2 μm (Fig. 5).

Figure 6 shows the thermogravimetric (TGA-DTA) spectra obtained for MCM-41(C10) over the temperature range 25 to 1,000 °C at a rate of 20 °C/min. Similar spectra were obtained for MCM-41(C_{12}) and MCM-41 (C_{14}), and the corresponding data were evaluated for the loss of water

Table 1 Structural and surface properties measured for unloaded MCM-41(C_N) samples

Sample	Morphology	Lattice parameter d_{100} (nm)	Pore diameter D_p (nm)	S_{BET} (m^2/g)	V (cm^3/g)	Loading capacity (wt%)
MCM-41(C_{10})	Spherical	3.1	1.4	869	0.51	29.4
MCM-41(C_{12})	Spherical	3.3	1.6	984	0.56	30.1
MCM-41(C_{14})	Rod-like	3.7	2.2	1149	0.75	33.2

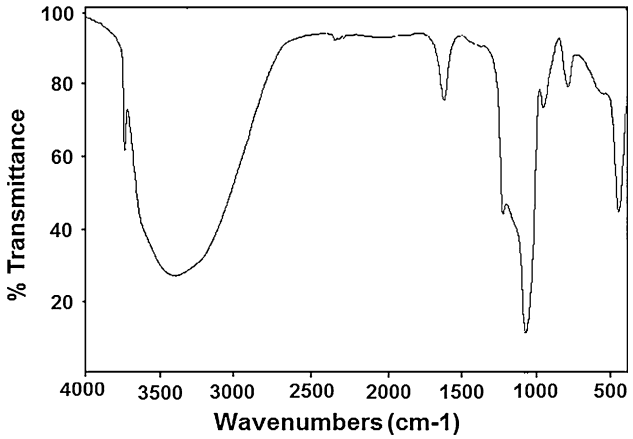

Fig. 3 FTIR spectra (4,000–400 cm^{-1}) of MCM-41(**C_{10}**) obtained using a KBr pellet (spectral resolution $\approx$ 4 cm^{-1})

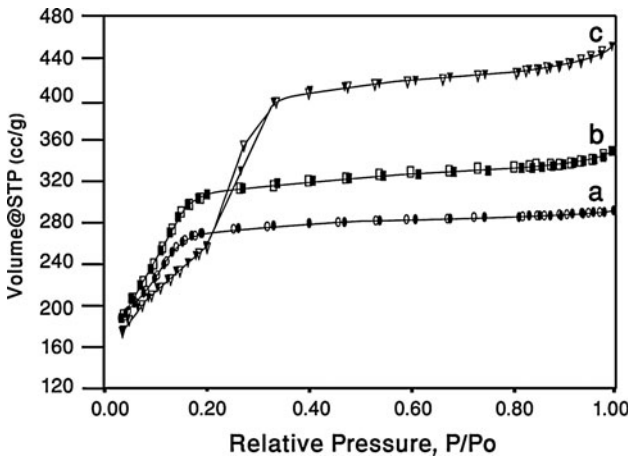

Fig. 4 Nitrogen adsorption/desorption isotherms for **a** MCM-41(C_{10}), **b** MCM-41(C_{12}), and **c** MCM-41(C_{14})

over different temperature ranges in light of what has generally been agreed to in the reported literature [31–39]. The results of this analysis are summarized in Table 2 for the three T-ranges: 25–300, 25–1,000, and 300–1,000 °C. In the first T-range (25–300 °C), the % mass loss is considered to result from desorption of water residing within the pores as bulk water plus water H-bonded to surface silanol groups. In contrast, the % mass loss within the 300–1,000 °C T-range is attributed to surface silanol groups decomposing into water, which was used to estimate the surface densities of pore surface silanol (Si–OH) hydroxyls. The total % mass loss over the T-range 25–1,000 °C expressed in terms of water is also indicated in the lower half of Table 2 for comparison with similar data that has been reported in the literature.

Within the 300–1,000 °C T-range, the number of moles of Si–OH groups (n_{Si-OH}) was estimated to be twice that of water lost according to

$$n_{Si-OH} = 2n_{w\,lost} = 2[(\%\,\text{mass lost})/(M_w \times SA)] \times 10^6 \mu\,\text{mol/m}^2 \quad (1)$$

where n_{Si-OH} is the number of micromoles of silanol groups per m^2 of MCM-41 pore surface (μ mol/m^2), % mass lost is the mass of water lost on heating above 300 °C in g water per g MCM-41, M_w is the molar mass of water (g/mol), and SA is the MCM-41 pore surface area per g of MCM-41 (m^2/g). The silanol number density (number of Si–OH hydroxyls per nm^2 surface,) is readily given by

$$N_{Si-OH} = 10^{-6} \times n_{Si-OH} \times L/10^{18}\text{nm}^{-2} \quad (2)$$

where L is Avogadro's number (6.022 $\times$ 10^{23} mol^{-1}).

The results listed in Table 2 indicate that the number density of surface Si–OH groups (lower half of the Table) decreases as the pore size or the overall pore surface area increases. For example, the number density goes down from 1.44 to 1.21 nm^{-2} on going from C_{10} to C_{14}. In units of μ mol/m^2, the respective decrease is from 2.39 down to 2.01 μ mol/m^2. The corresponding literature reported values for MCM-41(C_{16}) range from 1.6 to 4.5 μ mol/m^2 [31–40]. It should be stressed, however, that the variation in the reported measured number densities stems from the variability of many physical factors involved in the methods of preparation of MCM-41. These include variations in the methods of template removal, the types of surfactant templates used, the rates of heating up to the calcination temperature, the calcination temperatures used (typically $\geq$ 540 °C), the time periods spent at calcination, as well as the methods and rates of re-hydration. All of these lead to variations in the extent of pore surface hydration and, hence, to corresponding variations in the surface silanol densities measured.

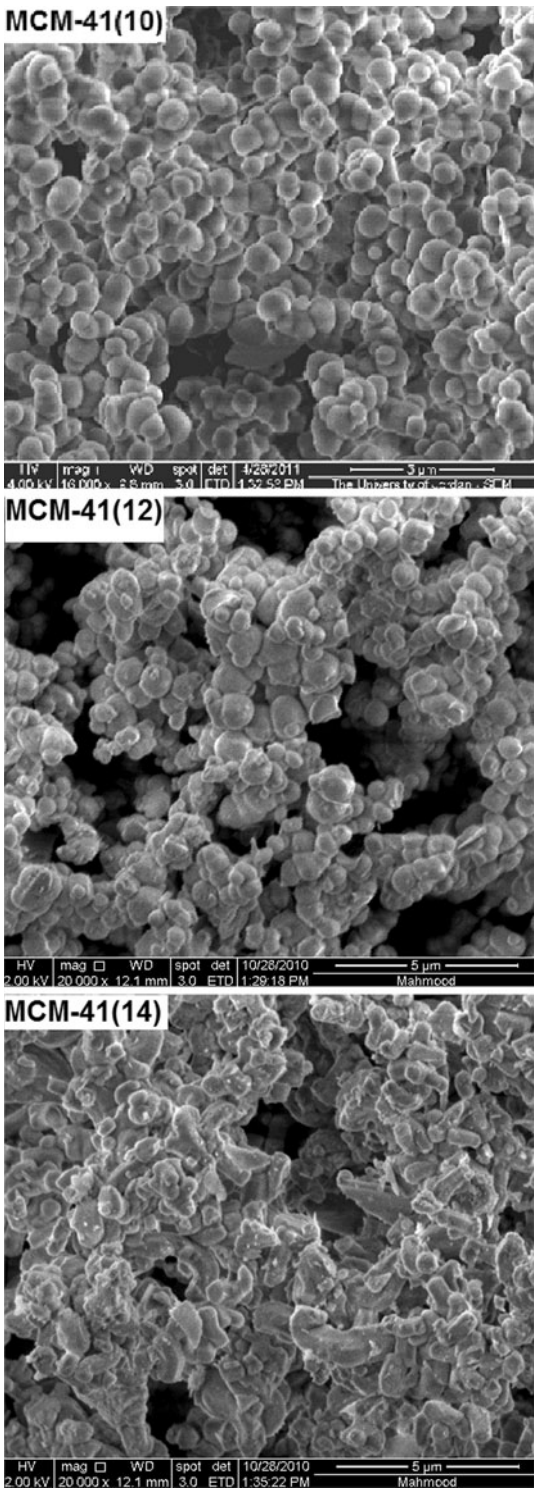

Fig. 5 SEM micrographs of unloaded MCM-41(C_{10}), MCM-41(C_{12}), and MCM-41(C_{14}) samples

3.2 Loading of the drug

Ephedrine was first liberated from its hydrochloride by reaction with sodium ethoxide in dry ethanol. Loading of free ephedrine was performed by the impregnation method using calcined MCM-41(C_N) samples. Loading of the drug into the mesoporous material was tested by nitrogen adsorption/desorption and IR-spectrometry. The loaded samples show a decrease in the pore diameter, pore size, and pore volume compared with those of the corresponding unloaded samples. In addition, the IR spectra of the loaded samples clearly show the presence of the drug in the loaded MCM-41(C_N) samples. The ephedrine-loading capacities of the MCM-41(C_N) samples were determined via UV–Visible spectrophotometry to be 29.4, 30.1, and 33.2% for MCM-41(C_{10}), MCM-41(C_{12}), MCM-41(C_{14}), respectively (Table 1).

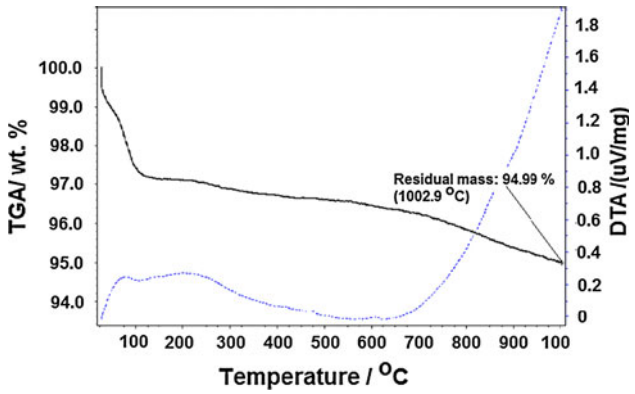

Fig. 6 Thermogravimetric (TGA-DTA) spectra obtained for MCM-41($\mathbf{C_{10}}$) within the temperature range 25–1,000 °C with a heating rate of 20 °C/min

3.3 Drug release profiles

The release profiles of ephedrine from the ephedrine-loaded MCM-41(C_N) disks into SBF buffer at pH 7.4 and 37 °C were measured in triplicates, and were averaged over the three experimental runs, for each of the C_N values. The data of each release profile were corrected for solution volume depletion, which results from sampling for measurement of ephedrine concentration in the release medium. These are depicted in Fig. 7 for the three MCM-41(C_N) materials: MCM-41(C_{10}), MCM-41(C_{12}), and MCM-41 (C_{14}), following normalization to 100% release.

Correction of the measured molar concentrations of ephedrine released into the buffer medium for solution volume depletion, on sampling, was conducted as follows. For a number of samples (n) consecutively drawn from the liquid release medium for analysis, the measured molar concentration of ephedrine (C_n) released into the medium at time (t_n) was corrected for liquid volume depletion using the following relation:

$$C_{n,corr} = C_n + (v/V_o) \sum_{i=1}^{i=n-1} C_i \quad (3)$$

Table 2 Surface silanol (Si–OH) group densities estimated for MCM-41(C_N); N = 10, 12 and 14, from thermogravimetric (TGA-DTA) data over the T-range 300–1,000 °C (lower half of the Table)

T-range = 25–300 °C			T-range = 25–1,000 °C		
(C_N)	% Mass lost	$n^a_{w\ lost}$ (mmol/g)	(CN)	% Mass lost	$n^a_{w\ lost}$ (mmol/g)
C_{10}	3.14	1.74	C_{10}	5.01	2.78
C_{12}	2.80	1.55	C_{12}	4.85	2.69
C_{14}	2.80	1.55	C_{14}	4.94	2.74

T-range = 300–1,000 °C

(C_N)	% Mass lost	$n^a_{w\ lost}$ (mmol/g)	SA[b] (m^2/g)	n^c_{Si-OH} (μ mol/m^2)	N^d_{Si-OH} (nm^{-2})
C_{10}	1.87	1.04	869	2.39	1.44
C_{12}	2.05	1.14	984	2.31	1.39
C_{14}	2.14	1.19	1,149	2.01	1.21

For the T-range 25–300 °C, only the number of moles of water lost on heating were listed (upper half of the Table) since only bulk water within the pores and water H-bonded to surface silanol groups are considered to desorb. The total water loss on heating from 25 to 1,000 °C is also listed (upper half of the Table) for reference

[a] $n_{w\ lost}$ = number of moles of water (mmol) lost on heating MCM-41 per 1 g MCM-41

[b] SA = surface area (m^2) of the mesoporous material per 1 g MCM-41

[c] n_{Si-OH} = number of micromoles of surface silanol lost on heating per 1 m^2 MCM-41

[d] N_{Si-OH} = number of silanol hydroxyls lost on heating due to decomposition into water

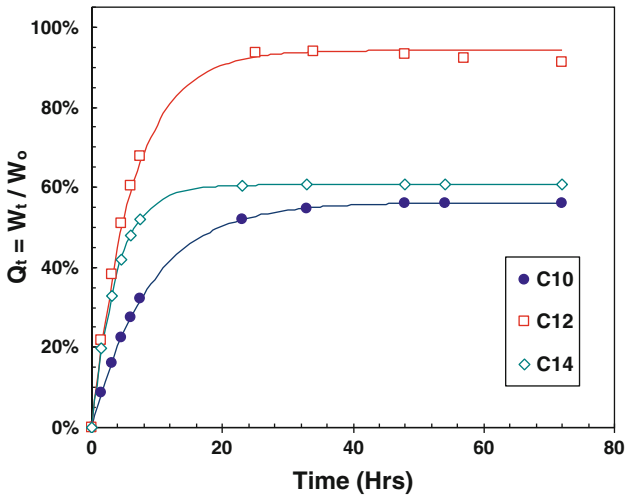

Fig. 7 Percent release profiles of ephedrine from ephedrine-loaded MCM-41(C_N) disks into SBF buffer solution at pH 7.4 and 37 °C, normalized to 100% release

where $C_{n,corr}$ is the molar concentration of drug released at time t_n corrected for liquid volume depletion on sampling for analysis, V_o is the initial volume of the release medium (250 mL SBF buffer solution), v the volume of each solution sample drawn for analysis (2.5 mL), and C_i is the measured drug concentration number-indexed for appropriate volume depletion correction; e.g., for a sample numbered (n; n ≥ 2) drawn from solution at time (t_n) for analysis, the index (i) runs from 1 (first sample) up to n-1. Using nonlinear regression analysis, the corrected molar concentration data ($C_{t,corr}$) against time (t) were fit to the *first order* drug release model [41] that is given by Eq. 4.

$$\%\,\text{Release} = C_{t,corr}/C_\infty = 1 - e^{-k\,t} \tag{4}$$

where $C_{t,corr} = C_{n,corr}$ at t_n, C_∞ is the maximum molar concentration of drug that can be released into the medium that is normalized to the initial solution volume (V_o), k is the corresponding release rate constant, and t is time in hours. Both C_∞ and k were used as floating parameters in nonlinear regression of % release against $(1 - e^{-k\ t})$, and the best parameter fits thus obtained were used to estimate the solid curve passing through the experimental release data shown in Fig. 7. Note that the % release data depicted in Fig. 7 were all normalized to 100% release. Normalization of % release to 100% release (Q_t) was carried out according to Eq. 5 below:

$$Q_t = W_t/W_o \tag{5}$$

where $W_t = C_{t,corr} \times V_o \times M$ is the mass of ephedrine released at time t, W_o is the mass of ephedrine that was initially loaded into the MCM-41(C_N) disk, while M is the molar mass of ephedrine.

The kinetic release parameters are tabulated in Table 3, which shows that the *first order* release constant (k) increases with the pore size of the MCM-41(C_N) host.

In contrast, the *HiguChi square root time* model based on Fickian diffusion [42] was also applied to the initial *first burst* given by the relation:

Table 3 Kinetic parameters of ephedrine release from ephedrine-loaded MCM-41(C_N) disks into SBF buffer at pH 7.4 and 37 °C

MCM-41(C_N) disk parameters				$Q_t = W_t/W_\infty = 1 - e^{-k\,t}$ (First order release model)				$Q_t = k_H\,t^{1/2} + c$, First burst	$Q_t = At^{1/2} + Bt$, A = Diffusion, B = Erosion
C_N	W^a (mg)	% Load	W_o^b (mg)	W_∞^c (mg)	Q_∞^d (%)	k ($hour^{-1}$)	MDT[e] (hour)	k_H ($hour^{-1/2}$)	A/B
C_{10}	296	29.4	86.7	44.3	56	0.11	8.9	0.16	1.6
C_{12}	326	30.1	98.0	89.4	92	0.16	6.2	0.32	4.1
C_{14}	281	33.2	93.4	51.5	60	0.26	3.8	0.21	32

[a] W = the mass of ephedrine-loaded MCM-41 disk

[b] W_o = the mass of ephedrine in the loaded MCM-41 disk

[c] W_∞ = the maximum mass of ephedrine released into the SBF buffer solution

[d] $Q_\infty = W_\infty/W_o$ = % load of ephedrine achieved, normalized to 100% release

[e] MDT = 1/k = Mean dissolution time (hours)

$$Q_t = k_H t^{1/2} + c \tag{6}$$

where k_H is the *Higuchi first burst* rate constant for initial drug release, which occurs relatively fast compared with subsequent release and c is a constant characteristic of the drug and host being formulated. Figure 8 shows a plot of Q_t against $t^{1/2}$ for ephedrine released by the three materials and the corresponding linear regression data fits are listed in Table 3. Unlike the *first order* rate constant (k), Table 3 shows that the value of the *Higuchi first burst* rate constant k_H is significantly higher for (C_{12}) than for (C_{10}) and (C_{14}), a trend which does not follow the change in pore size. In addition, the release appears to be *bimodal* where the *first burst* releases a major portion of the dose in about 6 h, while the remainder of the drug is more slowly released over a relatively longer period extending to some 20 h.

Further, the relative contributions of *diffusion* (A) and *erosion* (B) processes to ephedrine *first burst* release were estimated using nonlinear regression analysis of data

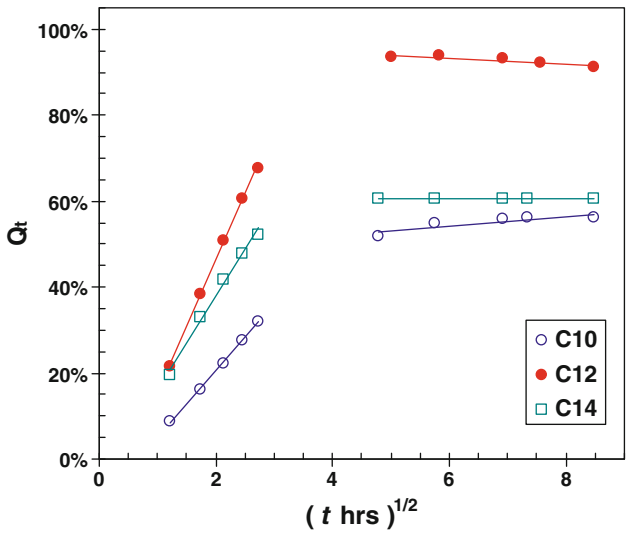

Fig. 8 % Release (Q_t) of ephedrine from ephedrine-loaded MCM-41(C_N) disks into SBF buffer solution at pH 7.4 and 37 °C plotted against $t^{1/2}$

according to the Kopcha's Empirical relation [43] given in Eq. 7 below:

$$Q_t = A\,t^{1/2} + B\,t \tag{7}$$

The A/B ratios thus obtained are listed in Table 3. It is evident from the A/B values (1.6, 4.1 and 32) for (MCM-41(C_{10}), MCM-41(C_{12}) and MCM-41(C_{14}), respectively), that diffusion is the principal mechanism for ephedrine release from MCM-41(C_N) disks, which becomes much more dominant as pore size increases.

Overall, the results of the investigation of loading into, and % release, of ephedrine from the three MCM-41(C_N) disks into SBF buffer at pH 7.4 and 37 °C, reveal the following observations:

(a) Loading of ephedrine into MCM-41(C_N) from dry ethanolic solutions of ephedrine is quite efficient, increasing slightly with an increase in pore size from MCM-41(C_{10}) to MCM-41(C_{14}), with the latter attaining a 33% load (Table 3).

(b) Among the three MCM-41(C_N) hosts, % release of ephedrine from MCM-41(C_{12}) appears to be the most efficient, approaching 92% of the loaded ephedrine in 20 h compared to only 56% for MCM-41(C_{10}) and 60% for MCM-41(C_{14}), over the same release time period (Fig. 7, Table 3).

(c) About 60% of the loaded ephedrine is released from MCM-41(C_{12}) in the first 6 h, while the remainder is released in the next 14 h (Fig. 7).

(d) The *first order* release rate constant (k), which was estimated from all data of the release profile, according to Eq. 4, consistently increases with pore size from 0.11 h^{-1} for MCM-41(C_{10}) up to 0.26 h^{-1} for MCM-41(C_{14}); the corresponding Mean Dissolution Times (MDT = 1/k) therefore decrease from 8.9 down to 3.8 h, respectively (Fig. 7, Table 3).

(e) In contrast, the *Higuchi first burst* rate constant (k_H), which was estimated over the first 6 h of release, Eq. 6, is clearly higher for MCM-41(C_{12}) than for

MCM-41 (C_{14}) (Table 3), a trend which does not follow the corresponding increase in pore size from MCM-41(C_{12}) to MCM-41(C_{14}), as would have been expected (Fig. 8, Table 3).

(f) Diffusion is the principal process governing ephedrine release, from MCM-41(C_N) pores (Table 3), which becomes much more dominant as pore size increases from MCM-41(C_{10}) to MCM-41(C_{14}).

It is not readily obvious why the *first burst* rate constant (k_H), of ephedrine released from MCM-41(C_N), is higher for MCM-41(C_{12}) than for MCM-41(C_{14}). For example, k_H rises from 0.16 $h^{-1/2}$ for MCM-41(C_{10}) to 0.32 $h^{-1/2}$ for MCM-41(C_{12}) then drops down to 0.21 $h^{-1/2}$ for MCM-41C_{14}). One physical difference that may contribute to this unexpected behavior may be attributed to the relatively longer and irregular pore channels observed in MCM-41(C_{14}), which may impart a relatively more steric hindrance to ephedrine release than those more ordered, yet shorter, pore channels observed in both MCM-41(C_{10}) and MCM-41(C_{12}). For example, it has been shown earlier (Table 1, Fig. 5) that MCM-41(C_{14}) exhibit irregularly-shaped rod-like particles which are roughly 2 μm long, compared with spherical MCM-41(C_{10}) and MCM-41(C_{12}) particles having 1.1 and 0.8 μm diameters, respectively. A similar behavior has earlier been observed for the release of captopril from MCM-41(C_{12}) into SBF buffer, which was found higher than the corresponding release from MCM-41(C_{16}), though the latter exhibited higher pore surface areas and higher captopril loading [44]. Again, MCM-41(C_{16}) particles were reported to be rod-like having pore channels ≈ 500 nm long, while those of MCM-41(C_{12}) were spherical with relatively short pore channels (120–150 nm).

No obvious trend was observed between the measured % release of ephedrine from MCM-41 mesopores and the corresponding silanol number densities, which have been estimated from thermogravimetric (TGA-DTA) analysis (Table 2).

4 Conclusion

Ephedrine loading into the mesoporous materials MCM-41(C_N) from dry ethanol solutions was observed to slightly increase with pore size, pore surface area or pore volume for the series MCM-41(C_{10}), MCM-41(C_{12}) and MCM-41(C_{14}). In contrast, the release of ephedrine from ephedrine-loaded MCM-41(C_N) disks, into simulated body fluid, was found most efficient for MCM-41(C_{12}) than for MCM-41(C_{10}) and MCM-41(C_{14}). The first burst release reached 60% of the drug load of MCM-41(C_{12}) in 6 h and 92% in 20 h. Therefore, MCM-41(C_{12}) is suggested as a good carrier for sustained release of ephedrine over many hours. Exploration of the in vitro release kinetics of ephedrine indicate that though drug-loading into MCM-41(C_N) materials from dry ethanol solutions slightly increase with pore size, the *first burst* release rate is not only a function of pore size, but is influenced by steric modulations restricting drug diffusion through the pores, which are imparted by extended pore channel lengths and varying particle morphologies.

Acknowledgments The authors gratefully acknowledge the financial support provided by the Deanship of Academic Research, University of Jordan, Amman, Jordan.

References

1. J.S. Beck, J.C. Vartuli, W.J. Roth, M.E. Leonowicz, C.T. Kresge, K.D. Schmitt, C.T.W. Chu, D.H. Olson, E.W. Sheppard, S.B. McCullen, J.B. Higgins, J.L. Schlenker, J. Am. Chem. Soc. **114**, 10834 (1992)
2. C.T. Kresge, M.E. Leonowicz, W.J. Roth, J.C. Vartuli, J.C. Beck, Nature **359**, 710 (1992)
3. A. Corma, Q. Kan, M.T. Navarro, J. Pérez-Pariente, F. Rey, Chem. Mater. **9**, 2123 (1997)
4. P. Horcajada, A. Ra'mila, J. Pe'rez-Pariente, M. Vallet-Regi', Microporous Mesoporous Mater. **68**, 105 (2004)
5. M. Vallet-Regi', A. Ra'mila, R.P. del Real, J. Pe'rez-Pariente, Chem. Mater. **13**, 308 (2001)
6. C.D. Nunes, P.D. Vaz, A.C. Fernandes, P. Ferreira, C.C. Romão, M.J. Calhorda, Eur. J. Pharmaceut Biopharm. **66**, 357 (2007)
7. W. Zenga, Q. Xue-Feng, Y. Jie, Z. Zi-Kang, Mater. Chem. Phys. **97**, 437 (2006)
8. K.C. Sousa, E.M. Souza, B. Sousa, Acta Biomater. **4**, 671 (2008)
9. Q. Fengyu, Z. Guangshan, H. Shiying, L. Shougui, D.Z. Jinyu Sun, Q. Shilun, Microporous Mesoporous Mater. **92**, 1 (2006)
10. N.K. Mal, M. Fujiwara, T. Yuko, T. Takahisa, M. Masahiko, Chem. Mater. **15**, 3385 (2003)
11. R. Aiello, G. Cavallaro, G. Giammona, L. Pasqua, P. Pierro, F. Testa, Stud. Surf. Sci. Catal. **142B**, 1165 (2002)
12. Y. Cao, Y. Bai, Z. Xia, Guisuanyan Xuebao **37**, 1570 (2009)
13. C. Gennara, P. Pierro, F. Salvatore, F. Testa, L. Pasqua, R. Aiello, Drug Delivery **11**, 41 (2004)
14. M. Vallet-Regi', F. Balas, D. Arcos, Angew. Chem. Int. Ed. **46**, 7548 (2007)
15. W. Xu, Y. Xu, D. Wu, Y. Sun, Stud. Surf. Sci. Catal. **170**, 861 (2007)
16. M. Manzano, V. Aina, C.O. Aréan, F.A. Balas, V. Cauda, M. Colilla, M.R. Delgado, M. Vallet-Regi, Chem. Eng. J. **137**, 30 (2008)
17. I.D. Carino, L. Pasqua, F. Testa, F. Aiello, F. Iemma, N. Picci, Drug Delivery **14**, 491 (2007)
18. C.D. Nunes, P.D. Vaz, A.C. Fernandes, P. Ferreira, C.C. Romao, M.J. Calhorda, Eur. J. Pharm. Biopharm. **66**, 357 (2007)
19. W. Zhao, A. Deng, D. Du, J. Zhang, Z. Li, H. Qin, J. Asian Nat. Prod. Res. **11**, 168 (2009)
20. C.A. Haller, L.B. Benowitz, N. Engl. J. Med. **343**, 1833 (2000)
21. A. Oyane, H. Kim, T. Furuya, K. Takuo, T. Kokubo, T. Miyazaki, T. Nakamura, J. Biomed. Res. Part A **65A**, 188 (2003)
22. T.R. Gaydhankar, V. Samuel, R.K. Jha, R. Kumar, P.N. Joshi, Mater. Res. Bull. **42**, 1473 (2007)
23. S. Wu, K. Song, J. Guan, Q. Kan, Bull. Mater. Sci. **34**, 979 (2011)
24. S. Ahmad, A. Ramli, J. Appl. Sci. **11**, 1178 (2011)

25. X.-D. Li, Q.-Z. Zhai, J. Iran, Chem. Soc. **8**, S1–S8 (2011)
26. O.A. Anunziata, M.L. Martinez, A.R. Beltramone, Materials **2**, 1508 (2009)
27. B. Lee, Y. Kim, H. Lee, J. Yi, Microporous Mesoporous Mater. **50**, 77 (2001)
28. K. Vidya, S.E. Dapurkar, P. Selvam, S.K. Badamali, N.M. Gupta, Microporous Mesoporous Mater. **50**, 173 (2001)
29. N.E. Poh, H. Nur, M. Nazlan, M. Muhid, H. Hamdan, Catal. Today **114**, 257 (2006)
30. Z. Hou, C. Zhang, C. Li, Z. Xu, Z. Cheng, G. Li, W. Wang, C. Peng, J. Lin, Chem. Eur. J. **16**, 14513 (2010)
31. P.K. Jal, S. Patel, B.K. Mishra, Talanta **62**, 1005 (2004)
32. J. Gallast, J. Goupilt, A. Vimont, J. Lavalley, J. Gilson, O. Miserques, Langmuir **25**, 5825 (2009)
33. I.G. Shenderovich, G. Bunkowsky, A. Schreiber, E. Gedat, S. Sharif, J. Albrecht, N.S. Golubev, G.H. Findenegg, H. Limbach, J. Phys. Chem. B **107**, 11924 (2003)
34. F. Kleitz, W. Schmidt, F. Shuth, Microporous Mesoporous Mater. **44–45**, 95 (2001)
35. F. Belhadj-Ahmad, E. Badens, P. Llewellyn, R. Denoyel, G. Charbit, J. Supercrit. Fluids **51**, 278 (2009)
36. M. Vallet-Regi, L. Ruiz-Gonzalez, I. Izquierdo-Barba, J.M. Gonzalez-Calbet, J. Mater. Chem. **16**, 26 (2006)
37. T. Benomar, L. Michelin, B. Lebeau, C. Marichal, Microporous Mesoporous Mater. **147**, 334–342 (2012)
38. X.Z. Zhao, G.Q. Lu, A.K. Whittaker, G.J. Millar, H.Y. Zhu, J. Phys. Chem. B **101**, 6525 (1997)
39. M. Odlyha, R.P.W. Scott, C.F. Simon, J. Thermal Anal. **40**, 1197 (1993)
40. P.R.S. Braga, A.A. Costa, J.L. de Mcedo, G.F. Ghest, M.P. de Sousa, J.A. Dias, S.C.I. Dias, Microporous Mesoporous Mater. **139**, 74 (2011)
41. T. Hekkila, H.J. Salonen, J. Tuura, N. Kumar, T.Y. Salmi, D.Y. Murzin, M.S. Hamdy, G. Mul, L. Laitinen, A.M. Kaukonen, J. Hirvonen, V.P. Lehto, Drug Deliv. **14**, 337 (2007)
42. T. Higuchi, J. Pharm. Sci. **52**, 1145–1149 (1963)
43. E. Chevalier, M. Viana, A. Artaud, S. Haddouchi, D. Chulia, Talanta **77**, 1545 (2009)
44. F. Qu, G. Zhu, S. Huang, S. Li, J. Sun, D. Zhang, S. Qiu, Microporous Mesoporous Mater. **92**, 1 (2006)